Defect structures mediate the isotropic-nematic transition in strongly confined liquid crystals†

Ioana C. Gârlea,*[a] and Bela M. Mulder[a]

Received Xth XXXXXXXXXX 20XX, Accepted Xth XXXXXXXXX 20XX
First published on the web Xth XXXXXXXXXX 200X **DOI: 10.1039/b000000x**

Using Monte Carlo simulations we study rod-like lyotropic liquid crystals confined to a square slab-like geometry with lateral dimensions comparable to the length of the particles. We observe that this system develops linear defect structures upon entering the planar nematic phase. These defect structures flank a lens-shaped nematic region oriented along a diagonal of the square box. We interpret these structures as a compromise between the 2-fold order of the bulk nematic phase and the 4-fold order imposed by the lateral boundaries. A simple Onsager-type theory that effectively implements these competing tendencies is used to model the phase behavior in the center of the box, and shows that the free-energy cost of forming the defect structures strongly offsets the transition-inducing effects of both the transverse and lateral confinement.

1 Introduction

Most applications of liquid crystals require these materials to be confined to small cells with boundaries specifically treated to orientationally "anchor" the mesogenic molecules, allowing the optical properties of the cell to be controlled[1] . In spite of the fact that the typical dimensions of these cells is continuously shrinking (current state-of-the-art displays employ $\sim 70\mu m$ pixels), commercially employed thermotropic mesogens typically have lengths of the order of a few nm's, so that a continuum description, in which the finite size of the particles is ignored, suffices to predict the relevant orientational patterns[2,3] . What happens, however, if the cell dimensions could be shrunk to the order of the particle size? This raises the interesting fundamental problem of liquid-crystalline behaviour in a regime where the particle size itself is a relevant parameter. What is the interplay between boundary effects and mutual interactions when these share the same length scale?

To experimentally address these questions, one would need either much smaller cells, or much longer particles. Since smaller cells are currently experimentally challenging to make, we can look to nature, which in principle provides us with filamentous protein aggregates in the micrometer length range. Prominent examples of such naturally occuring mesogens are the cytoskeletal polymers F-actin and microtubules, which both have lengths $\gtrsim 10\ \mu m$, and which *in vivo* are in fact generically confined to cellular (sub)volumes with dimensions comparable to that of these filamentous particles themselves[4, Chap. 16] . Indeed, recent experiments on F-actin in photolithographically created micrometer-sized slablike geometries show that intriguing ordering patterns can be observed, even at densities far below that of the bulk transition, that clearly reveal the tug-of-war between alignment with the lateral boundaries and mutual alignment[5,6] . Both these tendencies derive from the same source: the gain in translational entropy associated with reduction of excluded volume, either with the wall or between the particles, will, with increasing density, outweigh the decrease in orientational entropy due to ordering. However, using F-actin as a model rod-like particle has two main drawbacks: the in-situ polymerized filaments are likely to be widely polydisperse, and their persistence length of $\sim 16\mu m$ is itself of the order of both the filament length, as well as the confinement dimensions, making it likely that enthalpic effects associated with bending also come into play[6] . In another recent experimental work[7] genetically modified FD-virus particles were employed. The latter have the advantage of being both length-monodisperse and highly rigid. The length of the virus particles, however, is slightly less than a micron (880 nm), and hence still much smaller than the typical lateral system sizes of several 10s of microns. It is therefore also not surprising that the phenomenology of these experiments is well described by continuum theories as also reported there. These two examples indicate that the present experimental state of the art is, as yet, not fully able to probe the questions we pose in a well-controlled manner.

To properly address the regime in which a) the size of the confining cell is only a few times larger then the mesogens and b) the particles involved are non-deformable, we turn to particle-based simulations. These allow us to study these questions in a systematic manner in the simplest possible setting. We therefore consider systems composed of purely length-monodisperse and perfectly rigid hard rods. We focus on the same finite planar geometry of the experiments described in[5] . We thus consider in a cuboidal cell with a

[a] *FOM Institute AMOLF, Science Park 104, 1098XG Amsterdam, the Netherlands. E-mail: garlea@amolf.nl*

height significantly smaller than the length of the particles, and a square lateral cross-section, with side length a few times the length of the particles. We find that in this geometry the system undergoes a transition at a density $\sim 25\%$ below that of the the $3d$ bulk isotropic-nematic transition. The ordered phase is characterized by a lens-shaped nematic region oriented along one of the diagonals with $+1/4$ disclination lines in the corners, and, strikingly, flanked by two disclination walls emerging from the two corners of the other diagonal (for a general discussion on defects in liquid crystals please refer to[8,9]). This latter phenomenon is a clear signal of the non-trivial impact of finite particle-size.

Although, in the regime of comparable confinement size with mesogen length, earlier simulation studies have been reported for hard rods in a slab-like geometry[10,11] , these studies employed periodic boundary conditions in the lateral direction, and hence lack the requisite wall-bulk competition effect. Intriguingly, the experiments on vibro-fluidized assemblies of macroscopic metal rods (length $\sim$ 3 cm) in planar geometries[12] do consider the same geometry and with hindsight[12, Fig. 4a] also suggest the presence of the linear defect structures. In these experiments the length of the sides of the confining cell is less than 10 times the rod length and, hence, one could expect that finite particle size plays a role in the organization. However, these authors argued that the patterns they observed are in fact consistent with continuum Frank elasticity theory in the same geometry, where no defects other than the $+1/4$ point singularities in the corners of the diagonal ordering axis have been reported. Moreover, as a rigorous link between vibrated granular media to the statistical physics of thermally excited systems is lacking, we are at present unable to gauge how far these two systems are truly analogous. Very recent theoretical work by González-Pinto et al[13] considers a liquid crystal composed of rectangular particles confined to a 2d square nanocavity a few times larger than the particle length. In this case, however, the particles are restricted to two discrete orientations. Since these particles can only be aligned parallel to the walls, the formation of a lens-shaped nematic region aligned along the diagonal is impossible, precluding the phenomena reported here. Another very recent theoretical study by Chen[14] , which considers the solution of the $2d$ Onsager theory for infinitely thin needles confined to a square with sides 3 to 11 times larger than the particle length, does not seem to reproduce the linear defect structures, but rather suggests that the particles are at least partially aligned to the cross-diagonal as well, for which we find no evidence.

In order to illustrate the impact of the different factors at play, and to rationalize the result on the transition density we also discuss a microscopic toy-model, which captures part of the phenomenology of the observed isotropic-nematic transition.

2 Simulations

2.1 Methods

In our simulations we use rigid spherocylindrical particles of diameter D, which we adopt as our unit of length, and cylinder length L, covering a range of aspect ratios L/D from 10 - 38. The length of the square base of the cuboidal simulation volume was fixed to $W = 73$ units (see Fig. 1). In first instance, the height of the cell H was chosen to be either 3 or 6 units. In both these cases, the length of the particles is higher than the height, precluding rotations out of plane, thus defining a quasi-2d geometry. Next, we also considered the true $2d$ case, by setting $H = 1$. We take the z-axis of our reference frame along the height, and align the remaining two axes with the side walls. The mutual interactions between the particles, as well as the interaction with walls, are hard, and therefore fully specified by the purely geometrical condition of no overlap. The simulation method is a standard Metropolis Monte Carlo scheme[15] . For convenience, the particles are initially arranged in a regular pattern. We checked that the initial configuration has no effect on the final pattern, result being the same as for a random starting configuration. The most computationally demanding step in our algorithm is the inter-particle overlap check. In order to speed up the simulation we use a Verlet list scheme. This allows us to decrease the number of overlap checks per step, since only particles located in the vicinity of the particle that we attempt to move are considered not all the particles in the container. After the equilibration of the system (less than 10% of the total simulation time), we sample configurations that are independent. The distance, in Monte Carlo time, between two independent configurations is decided according to the mean diffusion time of particles over half the container size. We typically use 1000 configurations per simulation from which we extract the parameters of interest, averaging over these parameters to obtain the final results.

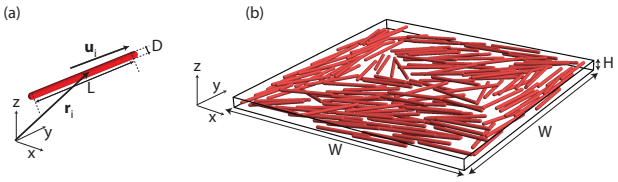

Fig. 1 Schematic of the simulated system: (a) A single particle and its size and configuration parameters. (b) The simulation box and its dimensions.

Apart from the standard second rank tensor order parameter $\mathbf{Q}$[9] , which provides a global measure of the order in our system and is used to monitor the equilibration of the system, we also employ a spatially resolved version, providing local

information on the orientational order, defined as

$$\mathbf{Q}^k = \frac{1}{\sum_i l_i^k} \left\langle \sum_i l_i^k \left(\frac{3}{2} \hat{\mathbf{u}}_i \otimes \hat{\mathbf{u}}_i - \frac{1}{2} \mathbf{1}_3 \right) \right\rangle \qquad (1)$$

where k labels a specific subvolume, i enumerates the particles in the system, each with its orientation specified by the unit vector $\hat{\mathbf{u}}_i$, l_i^k is the length of particle i inside the subvolume k, $\mathbf{1}_3$ is the 3d unit tensor, and the angular brackets denote equilibrium averaging. In practice, we found that height-spanning rectangular subvolumes of footprint 3.5×3.5 units, were an optimal compromise between resolution and computational effort. The use of the length l_i^k measured along the cylindrical part of the particles, instead of the more formally correct weighting by the volume fraction that particle i occupies in subvolume k, is a computationally convenient approximation, whose error is expected to be small for the highly elongated particles we consider. A frame-independent measure of the local degree of alignment is obtained by considering the largest positive eigenvalue λ_+^k of $\mathbf{Q}^k$, which ranges from 0 for a 3d fully disordered isotropic system, to 1 for a fully aligned system. The corresponding eigenvector $\hat{\mathbf{n}}_+^k$ of $\mathbf{Q}^k$, commonly called the director and defined up to its sign, points along the average direction of the preferred alignment.

2.2 Results

Changing the volume fraction of the particles –$\eta = \rho V_{part}$, with ρ the number density and $V_{part} = \pi D^2 L/4 + \pi D^2/6$ – we generically observe three types of orientational patterns within the simulation volume. All of them are in-plane structures, characterized by a smallest eigenvalue of $\mathbf{Q}$ of $\lambda_z \simeq -1/2$. For small volume fractions, we observe local alignment of the rods along the four side walls (fig 2 (a), (d), and (g)). Moving to the middle of the volume the degree of order rapidly falls off, with the center essentially fully isotropic in-plane corresponding to $\lambda_+ \simeq 1/4$. In this regime, the wall induced ordering appears dominant. At higher volume fractions, the system becomes smectic (see fig 2 (c), (f), and (i)), with the number of smectic layers dependent on the aspect ratio of the particles. Here the excluded-volume driven mutual alignment mechanism is able to overcome the barrier caused by disaligning the particles at the two side walls along the smectic director. At intermediate values of the volume fraction, the competition between the globally incompatible 4-fold ordering induced by the side walls and 2-fold nematic order due to mutual alignment leads to a compromise structure. We observe a lens-shaped nematic domain along one of the diagonals (see fig 2 (b)). This domain is flanked by two wall defect structures emanating from the corners of the other diagonal. As we approach these corners, the degree of order drastically decreases (see fig 2 (h)). Crossing the defect wall, the preferred direction of the particles makes a finite jump (see fig 2 (e)). The results in figure 2 (d-i) are obtained by averaging over the local orientation of the particles and the local degree of order of independent configurations from the same simulations. For the pattern characterized by the lens-shaped nematic we observe two configurations that are equivalent by symmetry, with the lens oriented along either of the two diagonals of the cell. Above the isotropic-nematic transition the pattern the systems randomly picks one of these two configurations. The patterns so-obtained are very stable with statistical errors typically two orders of magnitude smaller than the quantity being measured in each subvolume, except for the subvolumes that contain the disclinations, where the fluctuations are much more prominent. The observed states are generically independent of the initial conditions up to their symmetry, as it is possible to select the specific diagonal of order in the nematic state, or the layer orientation in the smectic state through a suitable bias in the initial arrangement of the particles. Depending on the initial configurations, we do sometimes observe particles trapped perpendicularly to the smectic layers, invariably next to the wall. We do not have enough statistics to conclude whether these transversely oriented particles are "trapped", or an equilibrium phenomenon such as first discussed in [16] .

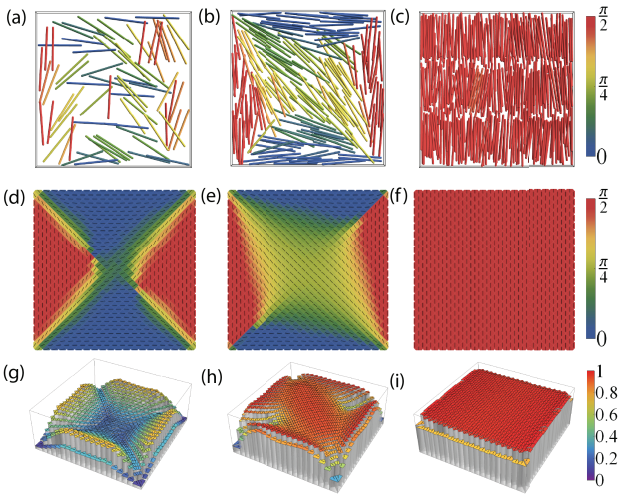

Fig. 2 Distinct states of the system: isotropic with wall alignment (a,d,g), lens-shaped nematic (b,e,h), and smectic(c,f,i). (a-c) Snapshots of typical configurations (top view). Color code corresponds to the minimum angle between the long axis of the rod and the **x** axis (scale bar on the right hand side). (d-e) Local orientation of the particles; Color code corresponds to the minimum angle between the local director $\hat{\mathbf{n}}_+^k$ and the **x** axis (scale bar on the right hand side).(g-i) Local degree of order of the system λ_+^k. All results presented in this figure are obtained for $H = 3$ and $L/D = 20$. Volume fractions are $\eta = 0.075$ for (a), (d), and (e), $\eta = 0.175$ for (b), (e), and (h), and $\eta = 0.3$ for (c), (f), and (i).

2.3 Disclination walls

To properly characterize these disclination walls, we define an angular deficit parameter δ on the lattice dual to our square mesh of subvolumes. If $\hat{\mathbf{n}}^1, \hat{\mathbf{n}}^2, \hat{\mathbf{n}}^3$ and $\hat{\mathbf{n}}^4$ are the four directors of the subvolumes that surround a point on the dual lattice in a fixed either clockwise- or anticlockwise order, then the angular deficit is defined as

$$\delta = min\angle\left(\hat{\mathbf{n}}^1, \hat{\mathbf{n}}^2\right) + min\angle\left(\hat{\mathbf{n}}^3, \hat{\mathbf{n}}^4\right), \qquad (2)$$

where the angle chosen is the minimal one obtained when the otherwise arbitrary signs of the director are varied. For a homogeneous nematic state this parameter vanishes. For the case of a gradual distortion, say a bend deformation, the parameter should vary smoothly. At any kind of singularity, however, the parameter provides a localized signal. As figure 3 shows, the parameter is high along the disclination walls, with a maximum in the corners, corresponding to the almost $\pi/2$ difference in angle caused by the wall induced ordering. As one moves along the diagonal, the particles on either side gradually splay away from the alignment at the wall, causing δ to decrease to a minimum, when the edge of the lens-shaped nematic domain is reached. Note that δ also picks up a signal at the $+1/4$ strength disclinations in the corners of the nematic domain, but this effect does not penetrate very far into the bulk.

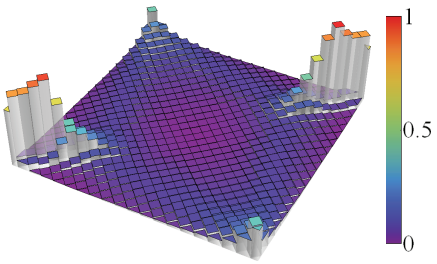

Fig. 3 Disclination parameter δ scaled by its maximum value π (color code given by the scale bar on the right). System parameters: $H = 3$, $L/D = 20$ and volume fraction $\eta = 0.175$.

2.4 Isotropic-nematic transition

To quantify the density dependence of development of order in our system, we study the value of the order parameter λ_+^{mid} of the subvolume exactly in the middle of the slab, i.e. the point farthest removed from the strong boundary-induced ordering at the side walls, which is high irrespective of the density. We tracked λ_+^{mid} for particles of aspect ratio $L/D = 15$, 20 and 25, for a range of volume fractions, spanning the isotropic, nematic and smectic regimes. In order to optimally isolate the influence of confinement and remove the known dependence of the mutual interactions on particle length, we scale all volume fractions by the value of the packing fraction at the bulk isotropic-nematic transition, which we obtain from the simulations of Bolhuis and Frenkel[17] , which defines the reduced volume fraction $\bar{\eta} = \eta/\eta_c\,(3d)$. Under this scaling the three curves indeed collapse reasonably well onto a single master curve (see Fig. 4).

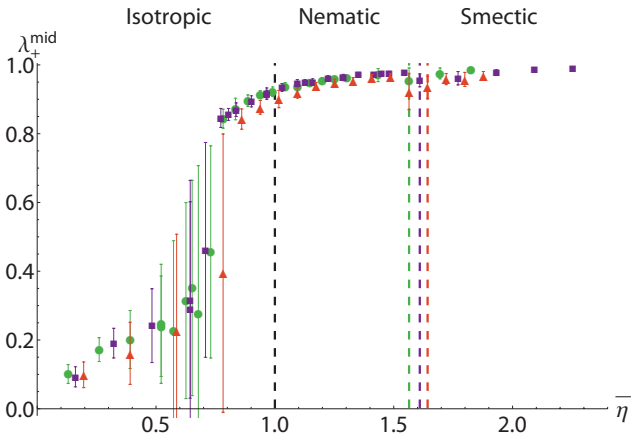

Fig. 4 Local degree of order λ_+^{mid} in the middle of the slab as a function of the density scaled by the bulk isotropic-to-nematic transition density. Error bars denote standard error in the mean. Simulation results at $H = 3$ for $L/D = 15$ (green circles), $L/D = 20$ (purple squares) and $L/D = 25$ (red triangles). The green, purple and red dashed vertical lines located between $\bar{\eta} = 1.5$ and 1.7 correspond to the nematic to smectic transition observed in the simulation in confinement for rods with $L/D = 15$, 20 and 25 respectively (from left to right). The black dashed line at $\bar{\eta} = 1.0$ marks the bulk isotropic-nematic transition.

At low volume fractions we expect the system to have an isotropic in-plane distribution, corresponding to $\lambda_+^{mid} \simeq 1/4$. The fact that the simulation data only reproduce this expected value at slightly higher volume fractions is due to the unavoidable undersampling of contributing configurations at low volume fractions. At a reduced volume fraction $\bar{\eta}_c \simeq 0.75$ we observe a strong first-order jump to a value $\lambda_+^{mid} \simeq 0.8$. As is usual in a finite system there are strong fluctuations in the transition region. Moreover, in this case the system is observed to repeatedly flip between the two symmetry equivalent preferred orientations along either of the diagonals. It is the latter effect that dominates the large error bars in the local degree of order in the transition region. Beyond the transition point, λ_+^{mid} increases, gradually saturating towards its maximal value $\lambda_+^{mid} \lesssim 1$, with only a small dip observed at reduced volume fraction $\bar{\eta}_s \simeq 1.5$, which marks the transition to the smectic state, in which the particles have to rotate from the box diagonal to either of the two shorter symmetry axes.

2.5 Results for $2d$ system

In order to check whether the effects reported above survive in the limit of a true $2d$ system, we also performed simulations by setting $H = 1$. In this system in which the particles are fully confined to the plane we again observe the same three distinct states: an isotropic phase with wall alignment in the vicinity of the boundary, a lens-shaped nematic and a layers arrangement. The density dependence of these states and the behavior of the order in the middle of the slab is very similar to the quasi-$2d$ case (cf. figure 5 (a)). Most importantly, the lens-shaped nematic is again stabilized by linear defects, which in this geometry are now pure line defects.

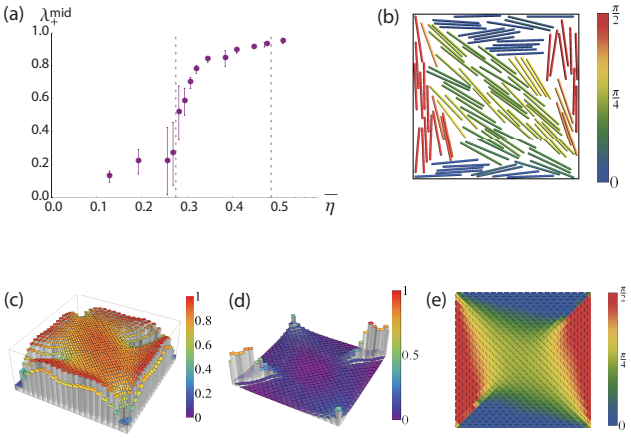

Fig. 5 Results for $2d$ system (box-height $H = 1$ and $L/D = 20$): (a) λ_+^{mid} versus $2d$ packing fraction $\eta \equiv \frac{N(\pi D/4 + L)}{W^2}$ (where N is the number of particles), showing the location of the I-N transition (left-hand dotted vertical line) and the $2d$ smectic transition (right-hand dotted vertical line). (b) snapshot at $\eta = 0.41$ (c) local order parameter (d) defect parameter (e) orientation pattern

3 Microscopic toy model

A notable result of our simulations is that the isotropic-nematic ordering transition takes place at a value of the density closer than expected to that of the homogeneous bulk. The results of Cosentino et al.[11] suggest that the transverse slab-like confinement strongly induces the in-plane ordering transition, which in their case happens at a reduced volume fraction $\bar{\eta}_c \simeq 0.25$, this value being fairly insensitive to the height of the slab, only increasing slightly when true $2d$ confinement is approached, where the nature of the transition changes to one driven by the condensation of bulk topological defects. Moreover, one also expects that by itself the pre-alignment effect caused by the interactions with the side walls would also facilitate the transition. Our results, however, indicate that, in the strong lateral confinement limit, nematic in-plane order is inevitably accompanied by the appearance of extended defect structures. These defects obviously carry a free-energy penalty, which potentially offsets the order-promoting effect of the transverse and lateral confinement.

To illustrate the effect of these competing mechanisms, we designed an Onsager-type[18] microscopic toy model that implements all the relevant effects, albeit in an effective manner. We thus consider a monodisperse system of highly elongated hard rods of length $L \gg D$. The mutual excluded volume at fixed relative orientations in this limit given by $E(\hat{\omega}, \hat{\omega}') = 2L^2 D \sin\gamma(\hat{\omega}, \hat{\omega}')$, where $\gamma(\hat{\omega}, \hat{\omega}')$ is the angle between two rods with orientations $\hat{\omega}$ and $\hat{\omega}'$. To mimic the confinement due to the finite height of the system, we impose a potential $\beta W_{\parallel}(\hat{\omega}) = \xi_{\parallel} P_2(\hat{\mathbf{z}} \cdot \hat{\omega})$, with P_2 the second-rank Legendre polynomial, and the prefactor is chosen to be $\xi_{\parallel} = \left(L^2/H^2\right)$, which matches the width of the Boltzmann weight of this potential to the maximal out-of-plane angle the rods can adopt, and any other non-dimensional factors are absorbed into the inverse temperature scale β. By symmetry, the effect of the side walls should be 4-fold symmetric in terms of the in-plane azimuthal angle φ. We implement this by adding the potential $\beta W_{\perp}(\hat{\omega}) = -\xi_{\perp} R_4^4(\hat{\omega}) \propto \cos(4\varphi)$, where $R_l^m(\hat{\omega})$ is a real spherical harmonic (see Supplemental Material[19] for details) and $\xi_{\perp}$ is a free parameter. Finally, we include a penalty associated with the defect structures, which we take to be proportional to the magnitude of in-plane order measured by the standard biaxial order parameter $T = \sqrt{\langle R_2^2 \rangle^2 + \langle R_2^{-2} \rangle^2}$, and whose strength is set by the free parameter ξ_d.This leads to the following free energy functional in terms of a normalized orientational distribution function $\psi(\hat{\omega})$:

$$\frac{\beta F[\psi]}{N} \equiv \Phi[\psi] = \int d\hat{\omega}\psi(\hat{\omega})\{\log\psi(\hat{\omega}) - 1\} + \rho L^2 D \int d\hat{\omega} \int d\hat{\omega}'\psi(\hat{\omega})\psi(\hat{\omega}')\sin\gamma(\hat{\omega}, \hat{\omega}') + \xi_{\parallel} \int d\hat{\omega}\psi(\hat{\omega}) R_2^0(\hat{\omega}) - \xi_{\perp} \int d\hat{\omega}\psi(\hat{\omega}) R_4^4(\hat{\omega}) + \xi_d \left\{ \left(\int d\hat{\omega}\psi(\hat{\omega}) R_2^2(\hat{\omega}) \right)^2 + \left(\int d\hat{\omega}\psi(\hat{\omega}) R_2^{-2}(\hat{\omega}) \right)^2 \right\}^{\frac{1}{2}},$$

where ρ is the number density. We numerically solve the minimization problem for this functional using a cumulant expansion technique, which results in a finite set of coupled equations for the expansion parameters, solved through a relaxation procedure (for details please consult the Supplemental Material[19]). In Fig. 6 we demonstrate that such a model readily fits the simulation results using the parameters $\xi_{\perp} = 0.07$ for $L/D = 15, 25$ and $\xi_{\perp} = 0.08$ for $L/D = 20$, and $\xi_d = 0.01$. The figure also shows that the term represent-

ing the transverse confinement, either by itself, or in conjunction with the one describing the coupling to the lateral walls, lowers the transition density to $\lesssim 50\%$ of the bulk value. The system, however, is very sensitive to the defect term, which, although small in amplitude, is sufficient to raise the transition density to the observed value.

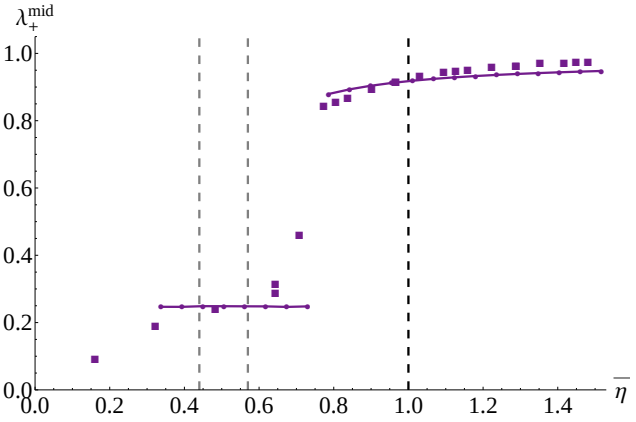

Fig. 6 Local degree of order λ_+^{mid} in the middle of the slab as a function of the density scaled by the bulk isotropic-to-nematic transition density. Simulation results at $H = 3$ for $L/D = 20$ (purple squares) and toy model fit (purple circles represent the result of the numerical minimization, whereas the purple line connecting them is just a guideline for the the eye) . The black dashed line at $\bar{\eta} = 1.0$ marks the bulk isotropic-nematic transition. The gray vertical lines correspond, from left to right, to the location of the transitions in the model for $\xi_d = 0$ and for $\xi_d = \xi_\perp = 0$.

4 Conclusion

We have shown that novel defect structures mediate the competition between mutual alignment and wall alignment in a confined system where finite particle size matters. We argue that such effects can generically be expected in uniaxially ordered phases whenever the geometry tries to impose "bend" distortions on the local director pattern on a spatial scale compared to the length of particles. In the case at hand this situation occurs in the corners of our simulation cell on the diagonal perpendicular to main axis of order. Whereas in a continuum description the resulting singularities can be fully localized to isolated points[7] , in the finite particle-size case these defects can be expected to have a spatial extent comparable to the length of the particles.

Whether the nature of the defect structures observed here – essentially a continuously decaying jump discontinuity in the director pattern– is in fact universal remains to be elucidated. It is therefore interesting to see what the implications of these findings are for other confinement geometries.

It will be interesting to see what happens if the height of the slab is increased, a regime we did not address in view of the significant computational costs involved. We do, however, believe that the defect walls will remain present. The experiments reported in[7] involving sub-micron long FD-virus particles in wells of several microns deep revealed that, even for systems in which the particles can in principle freely rotate out of plane, the observed structures are nevertheless strongly planar. This indicates that the planar alignment induced by the dominating top and bottom surfaces propagates throughout the whole sample, rendering the system effectively 2d, and hence susceptible to the defect structures described here. In the limit that the height equals the side length and the system geometry becomes cubic, we would predict that the central lens-shaped nematic region will align along a major diagonal of the cube with possible sheet-like defect structures emanating from the flanking vertices.

Our results should also be contrasted a number of complementary studies that have appeared of hard rods confined to $2d$ circular disks — simulations with homeotropic boundary conditions[20] , density functional theory[21] and very recently simulations with both homeotropic and planar boundary conditions[22] –, or a $3d$ spherical volume[23] with planar degenerate boundary conditions. In all these cases one expects to find as stable configurations either a single (homeotropic b.c.) or a polarly opposite pair of disclination points (planar b.c). These defects structures, however, are purely topological in origin, and well-described by continuum theory in the limit of strong anchoring and weak elastic effects (see e.g.[24]), and hence are not dependent on the finite size of the particles. The same arguably also holds for more complex situations, such as rods on the surface of a sphere[20,25] , squares on a sphere[26] , liquid crystals between concentric spherical shells[27,28] , liquid crystals confined to cylindrical pores[29] , liquid crystals on a toroidal surface[30] , or the complicated defect fields that can be designed using surface treated collids or surfaces[31–34] . This highlights the non-trivial nature of the stable linear defect structures we have observed.

Finally, experimental validation of these results clearly raises the challenge of producing sufficiently rigid monodisperse colloidal rods of the right dimensions and the ability to resolve orientational patterns at (sub)micron resolutions. Also, from a theory perspective, the proper approach is probably still lacking, as the "null" result (as far as the defects is concerned) of[14] suggest that we are dealing with a phenomenon that potentially requires a more powerful density functional theory, which takes into account interparticle correlations beyond the second virial coefficient level of the Onsager theory.

5 Acknowledgment

The work of ICG was supported by the FOM programme 110 "Spatial design of biochemical regulation networks". The work of ICG and BMM is part of the research programme of the Foundation for Fundamental Research on Matter (FOM), which is financially supported by the Netherlands Organisation for Scientific Research (NWO).

References

1 R. H. Chen, *Liquid Crystal Displays: Fundamental Physics and Technology (Wiley Series in Display Technology)*, Wiley, 2011, p. 520.
2 C. Tsakonas, A. J. Davidson, C. V. Brown and N. J. Mottram, *Applied Physics Letters*, 2007, **90**, 111913.
3 C. Luo, A. Majumdar and R. Erban, *Physical Review E*, 2012, **85**, 061702.
4 B. Alberts, A. Johnson, J. Lewis, M. Raff, K. Roberts and P. Walter, *Molecular Biology of the Cell*, Garland Science, 2007, p. 1392.
5 M. Soares e Silva, J. Alvarado, J. Nguyen, N. Georgoulia, B. M. Mulder and G. H. Koenderink, *Soft Matter*, 2011, **7**, 10631–10641.
6 J. Alvarado, B. M. Mulder and G. H. Koenderink, *Soft matter*, 2014, **10**, 2354–2364.
7 A. H. Lewis, I. Garlea, J. Alvarado, O. J. Dammone, P. D. Howell, A. Majumdar, B. M. Mulder, M. P. Lettinga, G. H. Koenderink and D. G. A. L. Aarts, *Soft Matter*, 2014, **10**, 7865–7873.
8 D. Demus and L. Richter, *Textures of Liquid Crystals*, Verlag Chemie, Weinheim, New York, 1978.
9 P. G. de Gennes and J. Prost, *The Physics of Liquid Crystals*, Clarendon Press, Oxford, 2nd edn, 1993.
10 M. Dijkstra, R. v. Roij and R. Evans, *Phys. Rev. E*, 2001, **63**, 051703.
11 M. Cosentino Lagomarsino, M. Dogterom and M. Dijkstra, *The Journal of Chemical Physics*, 2003, **119**, 3535–3540.
12 J. Galanis, D. Harries, D. L. Sackett, W. Losert and R. Nossal, *Phys. Rev. Lett.*, 2006, **96**, 028002.
13 M. González-Pinto, Y. Martínez-Ratón and E. Velasco, *Physical Review E*, 2013, **88**, 032506.
14 J. Z. Y. Chen, *Soft Matter*, 2013, **9**, 10921–10930.
15 D. Frenkel and B. Smit, *Understanding Molecular Simulation, Second Edition: From Algorithms to Applications (Computational Science)*, Academic Press, 2001, p. 664.
16 R. van Roij, P. Bolhuis, B. Mulder and D. Frenkel, *Phys. Rev. E*, 1995, **52**, R1277–R1280.
17 P. Bolhuis and D. Frenkel, *The Journal of Chemical Physics*, 1997, **106**, 666–687.
18 L. Onsager, *Annals of the New York Academy of Sciences*, 1949, **51**, 627–659.
19 I. C. Garlea and B. M. Mulder, *Supplementary Information to "Defect structures mediate the isotropic-nematic transition in strongly confined liquid crystals"*, 2014.
20 J. Dzubiella, M. Schmidt and H. Löwen, *Physical Review E*, 2000, **62**, 5081–5091.
21 D. de las Heras, E. Velasco and L. Mederos, *Physical Review E*, 2009, **79**, 061703.
22 D. de las Heras and E. Velasco, *Soft Matter*, 2014, **10**, 1758–1766.
23 Y. Trukhina and T. Schilling, *Phys. Rev. E*, 2008, **77**, 011701.
24 P. Prinsen and P. van der Schoot, *Physical Review E*, 2003, **68**, 021701.
25 M. A. Bates, *The Journal of chemical physics*, 2008, **128**, 104707.
26 Y. Li, H. Miao, H. Ma and J. Z. Y. Chen, *Soft Matter*, 2013, **9**, 11461–11466.
27 T. Lopez-Leon, V. Koning, K. B. S. Devaiah, V. Vitelli and A. Fernandez-Nieves, *Nature Physics*, 2011, **7**, 391–394.
28 S. R. Seyednejad, M. R. Mozaffari and M. R. Ejtehadi, *Physical Review E*, 2013, **88**, 012508.
29 R. Ondris-Crawford, G. Crawford, S. Zumer and J. Doane, *Physical review letters*, 1993, **70**, 194.
30 Y. Li, H. Miao, H. Ma and J. Z. Y. Chen, *RSC Adv.*, 2014, **4**, 27471–27480.
31 U. Tkalec, M. Ravnik, S. Čopar, S. Žumer and I. Muševič, *Science*, 2011, **333**, 62–65.
32 B. Senyuk, Q. Liu, S. He, R. D. Kamien, R. B. Kusner, T. C. Lubensky and I. I. Smalyukh, *Nature*, 2013, **493**, 200–205.
33 D. K. Yoon, Y. H. Kim, D. S. Kim, S. D. Oh, I. I. Smalyukh, N. A. Clark and H.-T. Jung, *Proceedings of the National Academy of Sciences*, 2013, **110**, 19263–19267.
34 A. Martinez, M. Ravnik, B. Lucero, R. Visvanathan, S. Žumer and I. I. Smalyukh, *Nature materials*, 2014, **13**, 258263.